Detailed modeling of local anisotropy and transverse K-u interplay regarding hysteresis loop in FeCuNbSiB nanocrystalline ribbons

Olivier Geoffroy, Nicolas Boust, Hervé Chazal, Sébastien Flury, James Roudet

RESEARCH ARTICLE | OCTOBER 27 2017

Detailed modeling of local anisotropy and transverse K_u interplay regarding hysteresis loop in FeCuNbSiB nanocrystalline ribbons

Special Collection: 23rd Soft Magnetic Materials Conference

Olivier Geoffroy; Nicolas Boust ; Hervé Chazal; Sébastien Flury; James Roudet

AIP Advances 8, 047712 (2018)
https://doi.org/10.1063/1.4993706

Detailed modeling of local anisotropy and transverse K_u interplay regarding hysteresis loop in FeCuNbSiB nanocrystalline ribbons

Olivier Geoffroy,[1] Nicolas Boust,[1,2] Hervé Chazal,[1] Sébastien Flury,[1] and James Roudet[1]
[1]*Univ. Grenoble Alpes, CNRS, Grenoble INP, G2Elab, F-38000 Grenoble, France*
[2]*Aperam Alloys Amilly, 45200 Montargis, France*

(Received 30 June 2017; accepted 31 July 2017; published online 27 October 2017)

This article focuses on the modeling of the hysteresis loop featured by Fe-Cu-Nb-Si-B nanocrystalline alloys with transverse induced anisotropy. The magnetization reversal process of a magnetic correlated volume (CV), characterized by the induced anisotropy K_u, and a deviation of the local easy magnetization direction featuring the effect of a local incoherent anisotropy K_i, is analyzed, taking account of magnetostatic interactions. Solving the equations shows that considering a unique typical kind of CV does not enable accounting for both the domain pattern and the coercivity. Actually, the classical majority CVs obeying the random anisotropy model explains well the domain pattern but considering another kind of CVs, minority, mingled with classical ones, featuring a magnitude of K_i comparable to K_u, is necessary to account for coercivity. The model has been successfully compared with experimental data.
https://doi.org/10.1063/1.4993706

I. INTRODUCTION

The nanocrystalline Fe-Cu-Nb-Si-B Finemet type alloys are characterized by a very low coercivity ($H_c < 0.5A/m$), comparable to the one featured by NiFe permalloys type crystalline alloys, or Cobalt based amorphous alloys ($H_c \cong 0.3A/m$), while exhibiting far greater spontaneous magnetization $J_s \cong 1.2T$ compared to 0.55 T for Co based amorphous or 0.75 T for Permalloys.[1] In addition, the low thickness (around 20 μm) of nanocrystalline ribbons, combined with a relatively high resistivity, dealing with metallic alloys, ($\rho \cong 115\ \mu\Omega cm$[1]), allow to obtain wound cores with low eddy current losses. As a result, this family is now widely used in middle frequency applications.

The remarkable magnetic specificity of those alloys, compared with classical crystalline ones, is that the thickness of a domain-wall (DW) is greater than the typical size D of a nanograin. As a result, the randomly distributed easy magnetization directions (EDs) featured by nanograins lead, at the scale of the DW, to an averaged effective anisotropy of amplitude $K_e \ll K_1$, K_1 denoting the magneto-crystalline constant relative to the nanocrystalline SiFe phase. More accurately, as explained by the random anisotropy model (RAM),[2] the magnetic correlation length obeys $L_{co} \cong \sqrt{A/\langle K_1 \rangle}$, with A the exchange stiffness and $\langle K_1 \rangle$ the mean fluctuation of the magneto-crystalline anisotropy averaged on a magnetic correlated volume (CV) L_{co}[3]. With D classically around 12 nm, vanishing $\langle K_1 \rangle$ is obtained. In this limit, K_{eff} is controlled by additional contributions, as the magnetoelastic anisotropy, explaining that the optimized alloys correspond to a resulting magnetostriction $\lambda_s \cong 0$, obtained when the magnetostriction of the residual amorphous phase balances the magnetostriction of the crystalline phase. The almost perfectly flat energetic landscape fulfilled by optimized ribbons allows developing coherent induced anisotropy, with magnitude denoted K_u in the following. K_u is obtained by means of dedicated annealing treatments, i.e. applying during annealing a magnetic field H_{an},[2] a high magnetic field[3] (i.e. $\mu_0 H_{an} > 1\ T$, usually provided by a superconducting magnet), or a tensile stress.[4–6] From an applicative point of view, the case of transverse K_u, i.e. ED perpendicular to

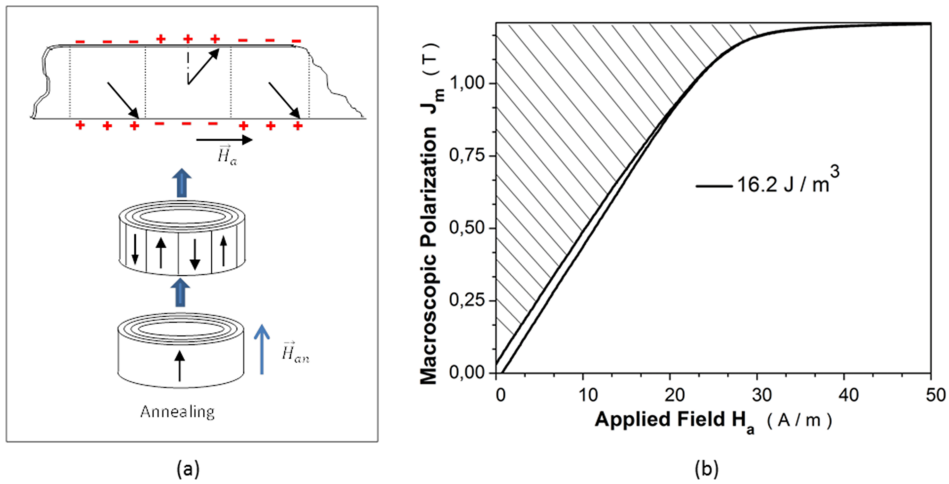

FIG. 1. (a): Schematic representation of the field annealing process and the induced strip domain structure obtained after annealing. The resulting coherent rotation magnetization mechanism is illustrated on a plane ribbon. (b): Half-loop obtained after transverse field annealing applied on a Nanophy® core. The anisotropy constant $\boldsymbol{K_u}$ is obtained measuring the dashed surface.

the direction of the applied field $\overrightarrow{H_a}$, is of great interest, leading to a practically linear behavior $J_m(H_a)$, J_m denoting the macroscopic polarization, with a slope adjusted by the parameters (magnitude of the field or stress) applied during the annealing treatment. This case is illustrated on Fig. 1.

According to the RAM, the macroscopic magnetic properties featured by nanocrystalline ribbons result from the statistical behavior of CVs, but most of the attention of the dedicated literature is centered on the modeling of the coercivity. The aim of this paper is to extend the analysis to the description of the hysteretic loop, through an analytical formalism. We'll focus on cores featuring transverse K_u, especially interesting regarding applications, as written above. From the modeling point of view, another positive point is that with K_u great enough, DWs displacements, with their inherent complexity, are negligible, compared to coherent rotation magnetization mechanism contribution.

This article develops previous results,[7] with a revised rigorous modeling of magnetostatic interactions (Sec. II B), a much more detailed study of the contribution of hard Correlated Volumes to the magnetization, with an accurate description of the different scales involved (Sec. III, introduction), completing analytic formulations (Sec. III B), illustrating the role of magnetostatics in the asymmetry featured by local loops (Sec. III C). The discretization of the continuous distribution of hard Correlated Volumes was improved, leading to much more satisfactory simulated macroscopic contribution (Sec. III D). At least, the approach leading to the analytic estimation of the mean deviation of the local easy axis is detailed in Appendix.

Wounded Nanophy® cores featuring typical composition $Fe_{73}Cu_1Nb_3Si_{16}B_7$ were provided by Aperam Alloys Amilly Company for experiments. Dimensions of the cores were outer diameter $D_{ext} = 3\,cm$, inner diameter $D_{in} = 2.5\,cm$ and height $h = 1\,cm$. Those cores were annealed under transverse field, as pictured on Fig. 1a, with typical duration one hour and annealing temperature 550 °C, under hydrogen atmosphere in the G2Elab furnace. After annealing, cores were characterized by fluxmetric measurements. Loops were performed at frequency $f = 0.5\,Hz$, i.e. in the quasi-static regime, a typical one being plotted on Fig. 1b. $K_u = 16.2\,J/m^3$ was determined measuring the dashed area delimited by the decreasing branch of the loop. This value will be used in the following for numeric evaluations.

II. MODELING REGARDING TYPICAL CVs

As explained in the introduction, the anisotropy experienced by CVs is mainly due to the coherent transverse anisotropy K_u. It is worth noting that if K_u was acting alone, the macroscopic law $J_m(H_a)$ would be perfectly linear, until saturation, with a reference susceptibility $\mu_0\,\chi_{ref} = {J_s}^2/(2\,K_u)$. As

shown on the experimental loop illustrated on Fig. 1b, the coercivity is non null, and usually attributed to a residual uncoherent anisotropy. For analytical convenience, this anisotropy is assumed to exhibit the same symmetry that the coherent one, i.e. uniaxial, K_i (subscript i as intrinsic) denoting its typical magnitude.

A. General formulations

The coexistence of those two anisotropies was extensively treated by Herzer et al.[2,6,8–10] According to Ref. 8, the effective anisotropy constant K_e obeys

$$K_e{}^2 = K_u{}^2 + K_i{}^2 \tag{1}$$

Following Herzer, we consider that the residual magneto-crystalline anisotropy, averaged over the scale of CVs, is the main origin for K_i for most of the CVs. Those CVs are thus considered "typical" and, obeying the RAM formalism, will be denoted CVRs in the following, devoted parameters being labelled with superscript R. According to Ref. 6, K_i^R verifies

$$K_i^R = 0.5\, x\sqrt{\beta K_1 K_u}(D/L_0)^3 \tag{2}$$

with x the crystalline volume fraction, $\beta = 0.4$ a factor reflecting the cubic symmetry of the crystals, $L_0 \cong 40\,nm$ the basic exchange length related to $K_1 = 8\,kJ/m^3$. This value corresponds to the composition of the nanocrystalline phase after crystallization, i.e. $Fe_{80}Si_{20}$ atomic [Ref. 11, fig. 2.10], the dependence of K_1 with composition being obtained from Ref. 12. Typical values corresponding to the anneals are $x \cong 0.7$, $D = 13\,nm$ [Ref. 11 Fig. 2.9], Ref. 13. With $K_u = 16\,J/m^3$, (2) leads to $K_i^R = 0.17\,K_u$. With (1) (replacing K_e and K_i by K_e^R and K_i^R), one obtains $K_e^R = 1.014\,K_u$. As a result, K_e^R is approximated to K_u.

Dealing with the ED resulting from the superposition of K_u and K_i^R, ones have to take in mind that, due to magnetostatic energy, the magnetization vector, at the scale of the magnetic domains, lies in the plane of the ribbon. As a result, we simplify the description, not considering the absolute easiest direction featured by a CV, but the easiest direction in the ribbon plane. The direction of this one can be described by a single variable, θ_{ED}, referenced to the direction of $\overrightarrow{H_a}$. Noting ε_R the mean deviation of the local ED, two kinds of CVs are thus considered, noted by subscript + or −, with $\theta_{ED}^+ = \pi/2 - \varepsilon_R$ and $\theta_{ED}^- = \pi/2 + \varepsilon_R$ (cf. Fig. 2), the polarizations being associated to angles θ_+ and θ_- (cf. Fig. 2). The energy featured by a CV is made up of the anisotropic contribution, with uniaxial symmetry, the Zeeman contribution (= applied field energy), and the magnetostatic one (long range interaction with surrounding CVs). Normalizing by K_u, the resulting reduced energy densities are thus written:

$$w_+ = k_e^R \cos^2(\theta_+ + \varepsilon_R) - 2h_a \cos\theta_+ + u_+ \tag{3}$$

$$w_- = k_e^R \cos^2(\theta_- - \varepsilon_R) - 2h_a \cos\theta_- + u_- \tag{4}$$

where $h_a = 0.5\,J_s\,H_a/K_u$ denotes the reduced applied field, $k_e^R = K_e^R/K_u$ the reduced anisotropy, (= 1), u_+ and u_- referring to the magnetostatic energies.

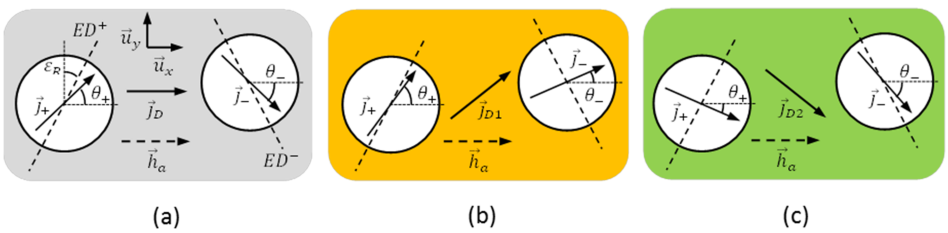

FIG. 2. Representation of each kind of typical CV (in white) interacting with the surrounding medium in a Weiss Domain (the EDs are dashed). (a): Configuration C_a; (b) and (c): Configuration C_b in two consecutive Weiss Domains D_1 and D_2. Dealing with C_b, the differences between polarizations $\vec{j}_+$ and $\vec{j}_-$ belonging to the same domain are strongly exaggerated for clarity.

B. Modeling of the magnetostatic energy

The magnetostatic energy is a key point in the description of soft granular systems, but is often neglected dealing with continuous media, as in Refs. 14–17. As pointed out by the pioneer work of Néel,[18,19] this should not be the case. We so present here a way to account for it.

It is worth noting that the CV must be considered immersed in a tridimensional environment. Indeed, even if for a magnetic domain, the magnetization vector is kept in the ribbon by the dipolar field, the characteristic length of a CV $L_{\text{co}} \cong \sqrt{A/K_e^R} \cong \sqrt{A/K_u} \cong 1\mu\text{m}$, with $A \cong 1.510^{-11} J/m$[20] is far small than the ribbon thickness, around 20 μm.

The modeling of interactions of a peculiar CV with the surrounding CVs is a very difficult challenge because of the great number of variables. A classical way to simplify the problem is to work in the frame of a mean field theory, as it will be done here. This kind of approach consists in replacing the surroundings CVs by an equivalent homogeneous medium (HM in the following), featuring a mean polarization $\langle \vec{J} \rangle_D = \langle \overrightarrow{J_{CV}} \rangle_D$, i.e.

$$\langle \vec{J} \rangle_D = \left(\vec{j}_+ + \vec{j}_- \right) x/2 + (1-x) \langle \vec{j}_a \rangle_D, \tag{5}$$

the subscript D indicating the magnetic domain the peculiar CV belongs to. $\vec{j}_{+(-)} = \cos\theta_{+(-)}\vec{u}_x + \sin\theta_{+(-)}\vec{u}_y$ denotes the polarization of each kind of CV (the reference system is indicated on Fig. 2), and $\langle \vec{j}_a \rangle_D$ the mean polarization of the amorphous phase, at the scale of the considered domain. The problem is further simplified, noticing that the SiFe phase is the most representative one ($x \cong 0.7$), and thus considering $x = 1$ in (5).

In addition, the HM features an effective susceptibility χ, assumed isotropic and uniform for analytical convenience. This means that the HM locally adapts to a local fluctuation of magnetization induced by a fluctuation of the ED at the scale of the given CV, with a resulting non uniform polarization $\overrightarrow{J_D} \neq \langle \vec{J} \rangle_D$. As a result, the vicinity of a peculiar CV acts as a shielding shell, reducing drastically the magnetostatic energies, compared to the situation featured by a HM with uniform polarization.

To quantify this effect, one starts from the reference state pictured on Fig. 3a where the polarization is uniform everywhere, i.e. $\overrightarrow{J_{CV}}$ (thin arrow) $= \langle \vec{J} \rangle_D$ (bold arrows), noticing that the directions of $\vec{H}_a$ and $\langle \vec{J} \rangle_D$ are considered different because $\langle \vec{J} \rangle_D$ is the average polarization at the scale of a magnetic domain, different from the macroscopic polarization $\overrightarrow{J_m} = \langle \langle \vec{J} \rangle_D \rangle$, where the external brackets indicate an average of $\langle \vec{J} \rangle_D$ on a significant number of domains.

As shown on Fig. 3b, because of local deviation of the ED, $\overrightarrow{J_{CV}}$ differs from $\langle \vec{J} \rangle_D$. Magnetostatic charges appear thus at the interface, inducing a dipolar field (thin lines on Fig. 3b), resulting in a variation (not pictured) of polarization in the HM.

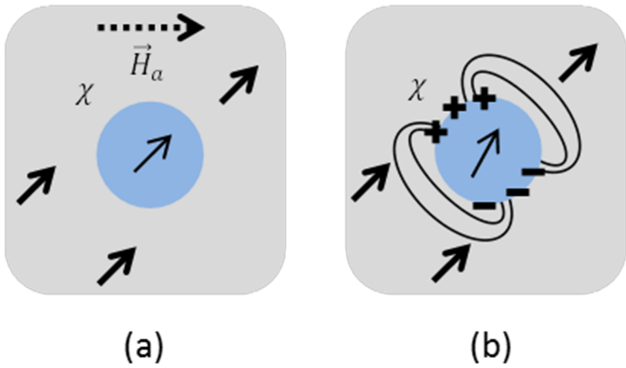

FIG. 3. (a): reference state: $\overrightarrow{J_{CV}} = \langle \vec{J} \rangle_D$; (b): Due to local fluctuation of ED, the direction of $\overrightarrow{J_{CV}}$ differs from the averaged polarization. As a result, magnetic charges appear at the interface, leading to a dipolar field outside the CV.

Noticing that the fields associated to the equilibrium resulting from the magnetic charges are variations with respect to the field $\vec{H}_a$ corresponding to the reference state (a), they will be denoted with prefix Δ in the following.

Following the general way indicated in Ref. 12, we obtain $\Delta\vec{H}_{CV} = \Delta\vec{H}^{CA}_{CV} + \Delta\vec{H}^{r}_{CV}$ where $\Delta\vec{H}^{CA}_{CV}$ and $\Delta\vec{H}^{r}_{CV}$ denote respectively the cavity and the reaction field contributions, according to the terminology popularized by Onsager.[21] In the present case, $\Delta\vec{H}^{CA}_{CV}$ and $\Delta\vec{H}^{r}_{CV}$ obey

$$\mu_0\,\Delta\vec{H}^{CA}_{CV} = \frac{1}{3+2\chi}\langle\vec{J}\rangle_D \quad \mu_0\,\Delta\vec{H}^{r}_{CV} = \frac{-1}{3+2\chi}\overrightarrow{J_{CV}} \tag{6}$$

As expected, $\Delta\vec{H}_{CV}$ is null if $\overrightarrow{J_{CV}} = \langle\vec{J}\rangle_D$

The torque exerted on the macrodipole associated to the central CV by the reaction field being null, the magnetostatic energy density U coupling the CV to the charges is reduced to

$$\mu_0 U = -\mu_0\,\Delta\vec{H}^{ca}_{CV}\overrightarrow{J_{CV}} = -\frac{1}{3+2\chi}\langle\vec{J}\rangle_D\,\overrightarrow{J_{CV}} = -\frac{1}{3+2\chi}\left\|\langle\vec{J}\rangle_D\right\| J_s \quad \cos\left(\theta_D - \theta_{CV}\right) \tag{7}$$

where $\theta_D - \theta_{CV}$ denotes the angle between $\langle\vec{J}\rangle_D$ and $\overrightarrow{J_{CV}}$. Eq. (7) provides a more rigorous evaluation of the magnetostatic energy than the one simply postulated in Ref. 7 by analogy with Ref. 13.

The determination of the effective susceptibility associated to the HM is of course a tricky task, the field induced by magnetic charges in the vicinity of the central CV being variable in amplitude and direction, and the intrinsic behavior featured by the surrounding CVs shaping the HM being hysteretic! Obviously, only numerical investigations are relevant to face this challenge accurately. In the frame of this first approach, analytical, we'll simply consider that the susceptibility χ_{ref} introduced above is a reasonable good order of magnitude, i.e. $\chi = {J_s}^2/(2\mu_0 K_u)$. One obtains $\chi \cong 36000 \gg 1$. As a result, $3+2\chi$ can be approximated by 2χ in (7), leading to the reduced magnetostatic energy

$$u_{CV} = -\left\|\langle\vec{J}\rangle_D\right\|\cos\left(\theta_D - \theta_{CV}\right) \tag{8}$$

C. Macroscopic law featured by CVRs

In our context, $\overrightarrow{j_{CV}}$ equals $\overrightarrow{j_+}$ or $\overrightarrow{j_-}$ and $\langle\vec{J}\rangle_D = (\overrightarrow{j_+} + \overrightarrow{j_-})/2$. After some elementary manipulations, (8) yields, neglecting constant terms, to the reduced magnetostatic energy featured by a CVR

$$u^R_+ = u^R_- = -0.5\cos\left(\theta_+ - \theta_-\right) \tag{9}$$

Inserting the magnetostatic contribution (9) in (3) and (4), and remembering that $k^R_e = 1$, leads to the reduced energies

$$w_+ = \cos^2\left(\theta_+ + \varepsilon_R\right) - 2h_a\cos\theta_+ - 0.5\cos\left(\theta_+ - \theta_-\right) \tag{10}$$

$$w_- = \cos^2\left(\theta_- - \varepsilon_R\right) - 2h_a\cos\theta_- - 0.5\cos\left(\theta_+ - \theta_-\right) \tag{11}$$

Equilibrium angles $\theta^e_{+(-)}$ are roots of equations $\partial w_{+(-)}/\partial\theta_{+(-)} = 0$. Differentiating (10) and (11) and introducing the new equilibrium variables $\theta_{av} = \left(\theta^e_+ + \theta^e_-\right)/2$, $\theta_d = \left(\theta^e_+ - \theta^e_-\right)/2$, one obtains the equilibrium equations:

$$\sin 2\left(\theta_{av} + \theta_d + \varepsilon_R\right) - 2h_a\sin\left(\theta_{av} + \theta_d\right) - 0.5\sin 2\theta_d = 0 \tag{12}$$

$$\sin 2\left(\theta_{av} - \theta_d - \varepsilon_R\right) - 2h_a\sin\left(\theta_{av} - \theta_d\right) + 0.5\sin 2\theta_d = 0 \tag{13}$$

Adding (12) and (13) leads to

$$\left(-\cos\theta_{av}\cos 2\left(\varepsilon_R + \theta_d\right) + h_a\cos\theta_d\right)\sin\theta_{av} = 0 \tag{14}$$

Two configurations solutions $C_i = \left(\theta_{av_i}, \theta_{d_i}\right)$ start to emerge, verifying

$$\theta_{av_a} = 0 \tag{15a}$$

$$\cos\theta_{av_b} = h_a\cos\theta_{d_b}/\cos 2\left(\varepsilon_R + \theta_{d_b}\right) \tag{15b}$$

It is noticeable that C_b entails no coercivity. From this point of view, configuration C_a seems to be more convenient to model the experimental macroscopic behavior. But another crucial point is that the y transverse component $\langle j^i_{tr}\rangle_D$ of the mean polarization in a Weiss domain associated to configuration $i = a$ *or* b obeys

$$2\langle j^i_{tr}\rangle_D = \sin(\theta_{av_i} + \theta_{d_i}) + \sin(\theta_{av_i} - \theta_{d_i}) \tag{16}$$

From (16) and (15a) $\langle j^a_{tr}\rangle_D = 0$ is obtained, as illustrated on Fig. 2a. This means that, at the scale of a Weiss Domain, there is no magnetostatic energy. The cost associated to domain walls in the strip structure classically observed by Kerr effect (see for instance Ref. 9, Fig. 5), schematically pictured on Fig. 1a, is thus not justified in this case. In other words, C_a cannot account for the strip structure. We underline that those deductions are very strong, being independent of the procedure used to model the magnetostatic interactions, the magnetostatic term being cancelled when adding (12) and (13) to obtain (14).

One completes the description of configurations C_a and C_b subtracting (13) to (12). This leads, besides relations (15a) and (15b), to

$$2h_a = (\sin 2(\varepsilon_R + \theta_{d_a}) - 0.5 \sin 2\theta_{d_a}) / \sin\theta_{d_a} \tag{17a}$$

$$2{h_a}^2 = \frac{1 + 0.5 \sin 2\theta_{d_b} / \sin 2\,(\varepsilon_R + \theta_{d_b})}{\dfrac{\cos^2\theta_{d_b}}{\cos^2 2\,(\varepsilon_R + \theta_{d_b})} + \dfrac{\sin 2\theta_{d_b}}{\sin 4\,(\varepsilon_R + \theta_{d_b})}} \tag{17b}$$

From (17a), one deduces the coercivity featured by configuration C_a, i.e.

$$h^a_c = 0.5 \sin 2\varepsilon_R \tag{18}$$

Fig. 4a shows the simulated loops associated to configurations C_a (Eq. 15a, 17a) (bold) and C_b (Eq. 15b, 17b) (dashed). We simulated with $\varepsilon_R = \pi/125$, for matching the experimental value $h^{ex}_c = 0.025$ and h^a_c. Apart from the disagreement already pointed out about the domain structure, the configuration C_a fails to reproduce the experimental mean slope and exhibits a crossing of the branches followed by the instability at point Q clearly unrealistic in regard to the experimental loop.

At the opposite, C_b exhibits a non null transverse polarization, as schematized on Fig. 2b and 2c. Moreover, as shown on Fig. 4b, $\langle j^b_{tr}\rangle_D$ decreases when h_a increases, agreeing well with the evolution of the magneto-optical contrast shown in Ref. 2, Fig. 2b. Lastly, Fig. 5a shows that θ_{d_b} is nearly null, leading with (9) to the cancellation of the local dipolar energy. As a result, C_b is more favorable, as Fig. 5b shows, comparing the mean equilibrium energies $\langle w_e\rangle_i = (w^e_+ + w^e_-)_i/2$.

Looking to typical CVs featuring residual incoherent anisotropy attributed to RAM, it is thus concluded that C_b is the only eligible configuration, which does not account for h_c.

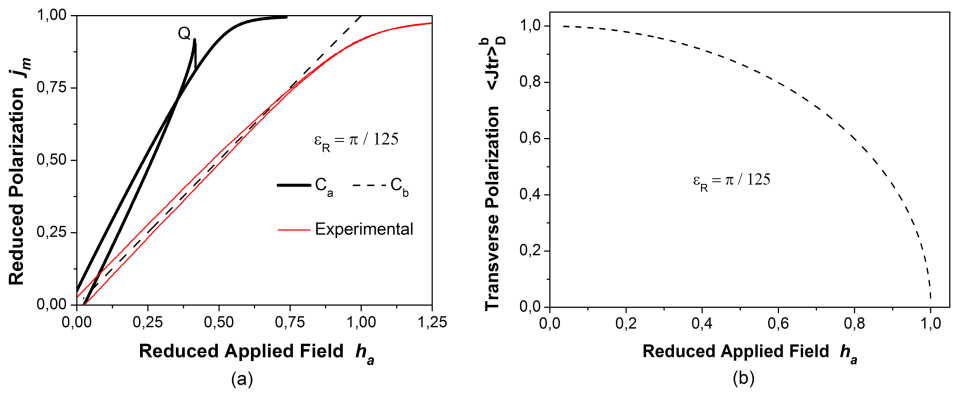

FIG. 4. (a): Simulated loops for configurations C_a (bold) and C_b (dashed), compared to the experimental loop (thin red). $\varepsilon_R = \pi/125$ was chosen for matching experimental value of h_c and the simulated one h^a_c. (b) Transverse polarization for configuration C_b.

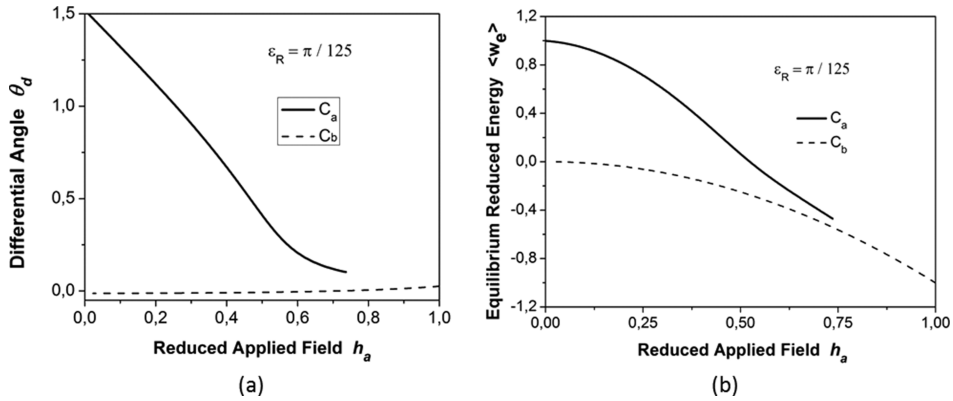

FIG. 5. (a). Evolution of differential angle θ_d for the two configurations (b). Comparison of energies for C_a and C_b.

It is noticeable that the existence of the configuration solution C_b is due to the coupling of θ_+ and θ_- through the magnetostatic term (see Eqs. 10 and 11). Without this term, a unique configuration would emerge, equilibrium angles θ_+^e and θ_-^e obeying the classical Stoner-Wolfarth formalism,[22] leading to a macroscopic behavior very comparable to the one featured by configuration C_a. This reinforces our initial statement, that is, independently of the way to model it, to take into account the magnetostatic term is of crucial importance.

III. INTRODUCING HARD CVs

According to previous conclusions, CVRs are considered obeying the anhysteretic C_b behavior. To account for h_c, some minority CVs (noted CVHs, as harder) have so to be involved, featuring a reduced uncoherent anisotropy $k_e^H > k_e^R$. Parameters characteristic of this new population will be labelled with superscript H. We'll describe at first how CVHs interact with CVRs and finally the impact of this cohabitation at the macroscopic scale. Between those extremes, different intermediate scales will appear. To facilitate the comprehension, we propose on Fig. 6 a global view of those different scales and corresponding polarisations notations, thick double arrows indicating the magnetostatic coupling.

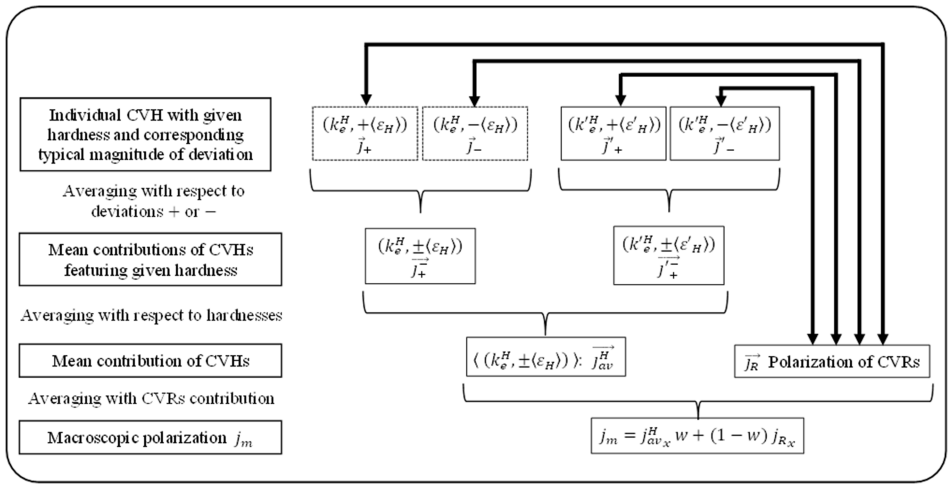

FIG. 6. Global synoptic of the different scales at which the magnetic behavior can be apprehended, with corresponding notations, starting from the local individual CVH until the macroscopic level. z denotes the hard CVs volumic fraction. In this symbolic scheme, k_e^H and $k_e'^H$ represent the actual continuous distribution of hardnesses. The distribution will in fact be approximated by 3 hardnesses (Sec. III D).

A. Equilibrium equations

To study the behavior of CVHs, the frame of the mean field theory introduced above is still followed. The major difference, compared with the case of CVRs, is about the link between the environment and the peculiar CV considered: Indeed, the CVHs volumetric part is expected to be only some % of the totality. The environment of a CVH can thus be nearly considered entirely made of CVRs, the mean properties of the corresponding HM being so disconnected from the central CVH considered now.

CVRs feature configuration C_b and for simplicity the corresponding differential angle is assumed to be null, according to Fig. 5a. As a result, all the CVRs belonging to a Weiss Domain exhibit the same polarization, described by a single angular variable and denoted $\vec{j}_R = \cos\theta_R\vec{u}_x + \sin\theta_R\vec{u}_y$. It is obtained with (15b) $\cos\theta_R = h_a/\cos 2\varepsilon_R$, that is, neglecting $\cos 2\varepsilon_R$:

$$\cos\theta_R = h_a \tag{19}$$

For analytical convenience, in the frame of the description of the surrounding medium of a peculiar CVH, $\vec{j}_R$ will be assimilate with $\vec{j}_D$, neglecting the influence of the minority CVHs contribution. It is thus obtained $\|\langle\vec{j}_D\rangle\| = 1$ and $\theta_D = \theta_R$, yielding with (8) to the magnetostatic energy associated to a CVH

$$u^H_{+(-)} = -\cos\left(\theta_R - \theta_{+(-)}\right) \tag{20}$$

Equations (19) and (20) are inserted in (3), (4), replacing $k^R_e = 1$ by k^H_e and ε_R by ε_H, yielding to:

$$w_+ = k^H_e\cos^2(\theta_+ + \varepsilon_H) - 2\cos\theta_R\cos\theta_+ - \cos(\theta_R - \theta_+) \tag{21}$$

$$w_- = k^H_e\cos^2(\theta_- - \varepsilon_H) - 2\cos\theta_R\cos\theta_- - \cos(\theta_R - \theta_-) \tag{22}$$

This leads, after differentiation, to the equilibrium equations

$$3\cos\theta_R\ \sin\theta^e_+ - \cos\theta^e_+\ \sin\theta_R = k^H_e\ \sin 2\ (\theta^e_+ + \varepsilon_H) \tag{23}$$

$$3\cos\theta_R\ \sin\theta^e_- - \cos\theta^e_-\ \sin\theta_R = k^H_e\ \sin 2\ (\theta^e_- - \varepsilon_H) \tag{24}$$

B. About irreversibility

A key point is to evaluate the typical hardness required to allow irreversibility, this point conditioning the possibility to account for dissipation and thus for coercivity. We'll denote θ^j_+ a critical angle (subscript j as jump). θ^j_+ verifies (23), being a peculiar equilibrium angle, and the additional relation $\frac{\partial^2 w_+}{\partial\theta_+{}^2}\Big)_{\theta^j_+} = 0$. Denoting θ^j_R the peculiar value of θ_R at which the jump occurs, it is thus obtained

$$6\cos\theta^j_R\ \sin\theta^j_+ - 2\cos\theta^j_+\ \sin\theta^j_R = 2k^H_e\ \sin 2\left(\theta^j_+ + \varepsilon_H\right) \tag{25}$$

$$3\cos\theta^j_R\cos\theta^j_+ + \sin\theta^j_+\sin\theta^j_R = 2k^H_e\cos 2\left(\theta^j_+ + \varepsilon_H\right) \tag{26}$$

Similar expressions are obtained for θ^j_-, replacing ε_H by $-\varepsilon_H$.

θ^j_R given, to determine the corresponding expression of k^H_e, one can express the combined equation $(25)^2 + (26)^2$. This leads to the second order equation

$$\left(2W + V^2\right)x^2 + 2\left(V\left(U - 4k_e^{H^2}\right) - W\right)x + \left(U - 4k_e^{H^2}\right)^2 = 0 \tag{27}$$

Where $= \cos^2\theta^j_+$; $V = 3\left(\sin^2\theta^j_R - 9\cos^2\theta^j_R\right)$; $U = 1 + 35\cos^2\theta^j_R$; $W = 40.5\sin^2 2\theta^j_R$.

The minimum value $k^H_{e\ lim}$ to obtain a jump for a given θ^j_R corresponds to the cancellation of the discriminant of Eq. (27), that is

$$k^H_{e\ lim} = \frac{1}{2}\sqrt{\frac{U\sqrt{2W + V^2} + UV - W}{\sqrt{2W + V^2} + V}} \tag{28}$$

Injecting (28) in (27), one obtains the corresponding critical angle

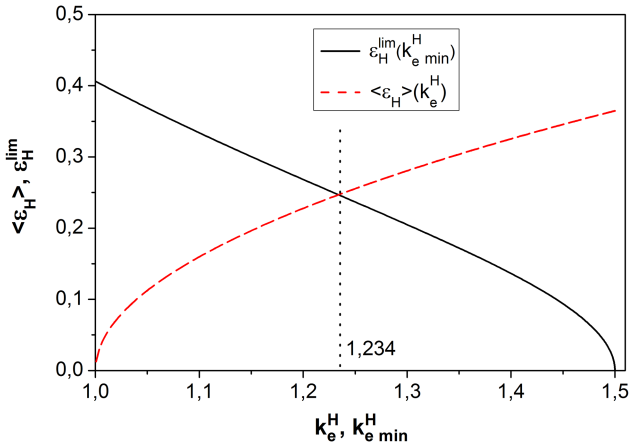

FIG. 7. Graphical determination of the representative minimum hardness to allow irreversibility determined as the intersect of the curve describing the intrinsic relation $\varepsilon_H^{lim}\left(k_{e\,lim}^H\right)$ and the curve $\langle\varepsilon_H\rangle\left(k_e^H\right)$ associated to representative CVHs.

$$\cos^2\theta_+^j = \frac{U - 4k_{e\,lim}^{H\,2}}{\sqrt{2W + V^2}} \tag{29}$$

The corresponding deviation ε_H^{lim} is obtained injecting (28) and (29) in (26), and obeys finally

$$\varepsilon_H^{lim} = \text{Arccos}\sqrt{\frac{W}{\sqrt{2W + V^2}V + 2W + V^2}} \tag{30}$$

The curve $\varepsilon_H^{lim}\left(k_{e\,lim}^H\right)$ is plotted on Fig. 7 (continuous black). As expected, this curve is decreasing, a little value of k_e^H requiring a great deviation of the ED to maintain the anisotropy energy at a sufficient level to allow irreversibility.

Nevertheless, the question of the representability of a couple $\left(k_{e\,lim}^H, \varepsilon_H^{lim}\right)$ has now to be asked. Indeed, from a general point of view, the effect of a given hardness k_e^H should ideally be rendered averaging the contributions considering all deviations ε_H, according with the distribution $\varepsilon_H\left(k_e^H\right)$. Regarding the complexity of the task, we simplify, considering that the couple $\left(k_e^H, \langle\varepsilon_H\rangle\left(k_e^H\right)\right)$ is representative of the actual average. In the present context, this means that among all couples $\left(k_{e\,lim}^H, \varepsilon_H^{lim}\right)$, the one featuring $\varepsilon_H^{lim} = \langle\varepsilon_H\rangle\left(k_{e\,lim}^H\right)$ is relevant, others playing a role of curiosities weightless. It is thus necessary to complete the study looking to mean properties of deviation to provide a comprehensive overview of the *representative* minimum value ${}_e^H k_{lim}^{re}$ to obtain a jump. This is done in the Appendix. Particularizing notations to the present context, the mean deviation $\langle\varepsilon_H\rangle$ for a given intrinsic hardness k_i^H obeys

$$\langle\varepsilon_H\rangle = 0.25\pi \tanh 0.45 k_i^H \tag{31}$$

Inserting (1) (replacing K_e by K_e^H and K_i by K_i^H) in (32), one obtains

$$\langle\varepsilon_H\rangle = 0.25\pi \tanh 0.45\sqrt{\left(k_e^{H^2} - 1\right)} \tag{32}$$

The corresponding curve is plotted on Fig. 7 (dashed red). In the context of irreversibility, the *representative* minimum hardness ${}_e^H k_{lim}^{re}$ to obtain a jump is so determined by the intersect of $\varepsilon_H^{lim}\left(k_{e\,lim}^H\right)$ and $\langle\varepsilon_H\rangle\left(k_e^H\right)$ curves, as shown on Fig. 7. One obtains ${}_e^H k_{lim}^{re} \cong 1.234$. With (1), this leads to an intrinsic anisotropy ${}_i^H k_{lim}^{re} \cong 0.72\, K_u$. In the peculiar case featured by the experimental loop pictured on Fig. 1, one obtains ${}_i^H k_{lim}^{re} \cong 4.3\, K_i^R$. As expected, the population of minority CVs considered has to be harder that the majority CVRs studied at first, to account for coercivity. This is consistent with our scheme.

Dealing with representative CVHs, we'll consider in the next only couples $\left(k_e^H, \varepsilon_H\right)$ *featuring* $\varepsilon_H = \langle \varepsilon_H \rangle \left(k_e^H\right)$ *given by (32).*

C. Local loops

The magnetic behavior featured by CVHs immersed in CVRs is deduced from Eqs. (23) and (24). Dealing with CVHs+, we consider $(23)^2$, obtaining the second order equation

$$Ay^2 - 2By + C = 0 \tag{33}$$

Where $y = \cos\theta_R$ $A = 1 + 8\sin^2\theta_+^e$ $B = 3\,k_e^H \sin\theta_+^e \sin 2\left(\theta_+^e + \varepsilon_H\right)$ $C = k_e^{H^2} \sin^2 2\left(\theta_+^e + \varepsilon_H\right) - \cos^2\theta_+^e$ θ_+^e given, two roots are obtained, verifying

$$\cos\theta_R^a = \left(B + \sqrt{B^2 - AC}\right)/A \qquad \cos\theta_R^b = \left(B - \sqrt{B^2 - AC}\right)/A \tag{34}$$

Ones has to take in mind that, according to the strip structure, $\theta_R \in [0, \pi]$ or $\theta_R \in [\pi, 2\pi]$, depending on the Weiss Domain the CVH belongs to. We'll arbitrary consider $\theta_R \in [0, \pi]$. $\cos\theta_R^a$ and $\cos\theta_R^b$ been known, θ_R^a and θ_R^b are so entirely determined. Considering the input variable $\theta_+^e \in [0, 2\pi]$, one obtains the relevant solution θ_R checking what root θ_R^a or θ_R^b verifies (24). Remembering that $h_a = \cos\theta_R$ (Eq. 20), one obtains the local loop featured by CVHs+ plotting the points $(h_a, \cos\theta_+^e)$. The same approach will apply to CVHs−, replacing θ_+^e by θ_-^e and ε_H by $-\varepsilon_H$ in parameters A, B and C.

k_e^H given, the corresponding averaged loop is obtained plotting the points $(h_a, j_+^- = (\cos\theta_+^e + \cos\theta_-^e)/2)$. At this stage, h_a is the entrance variable. This means that it is necessary to interpolate corresponding values of $\cos\theta_+^e$ and $\cos\theta_-^e$. This will impact the strategy we'll adopt looking to macroscopic scale (Sec. III D).

1. $k_e^H \cong k_{e\,lim}^H$

Fig. 8a and 8b illustrate the case $k_e^H = 1.23$ $\left(\cong {}_e^H k_{lim}^{re}\right)$. The loops associated to each kind of CVH are plotted on Fig. 8a. They are anhysteretic, as expected, the double arrows indicating that the same route is travelled increasing or decreasing the field. Logically, the averaged loop is anhysteretic too. Nevertheless, the thin arrows point the approach of instability which will lead to irreversibility for an infinitesimal increase of k_e^H.

A non-trivial characteristic is the negative slopes observed towards saturation ($|h_a| > 0.81$), looking to individual behaviours (Fig. 8a). It is explained noticing that the natural tendency of the local polarization is to proximate the ED. But the magnetostatic cost being related to $\theta_D - \theta_{CVH}$ (see Eq 20), the local Polarization has to proximate $\vec{j}_D$ too. As a consequence, different stages occur, i.e., considering CVH+ for illustrating (see Fig. 9):

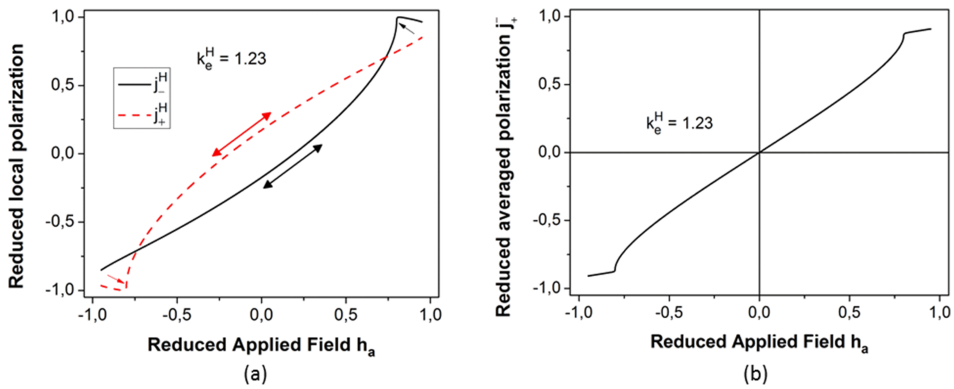

FIG. 8. (a). Local anhysteretic loops characteristics of CVHs featuring $k_e^H = 1.23$ (b). Corresponding averaged anhysteretic loop.

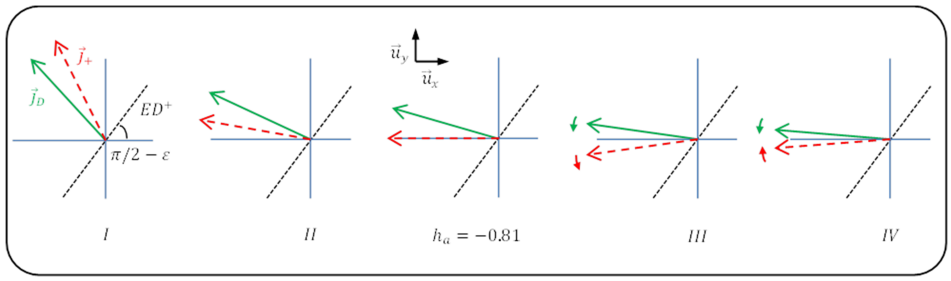

FIG. 9. Qualitative explanation of the negative slope observed for $|h_a| > 0.81$ on the loops illustrated on Fig. 8a: illustration of the evolution of $\vec{j}_+$ towards negative saturation, $|h_a|$ increasing from I to IV. The differences of orientations are amplified for visibility.

Stage I: $\vec{j}_+$ is late with respect to $\vec{j}_D$, looking towards the easy angle $\theta_{ED} = \pi/2 - \varepsilon$;
Stages II, III, IV: $\vec{j}_+$ is in advance, looking towards the approaching easy angle $\theta_{ED} = 3\pi/2 - \varepsilon$;
We now focus on stages II and III. The situation can be explained considering for simplicity that the evolution of h_a is small enough in these stages to neglect the variation of the Zeeman contribution in regard of the magnetostatic and anisotropic energy variations (note that the evolution of h_a is anyway partially accounted trough the evolution of θ_D, impacting the magnetostatic term). As a result, optimizing the energetic compromise between anisotropic contribution and magnetostatic one leads to the increase of θ_+^e with θ_D, that is
Stage II: θ_+^e increasing with θ_D (and so with $|h_a| = |\cos\theta_D|$), $|j_x^+| = |\cos\theta_+^e|$ increases too, so long as $\theta_+^e < \pi$;
Stage III: θ_+^e being greater than π, the increase of θ_+^e with θ_D leads to a decrease of $|j_x^+|$ with $|h_a|$;
Stage IV: The energetic compromise is here essentially driven by the anisotropic term and the Zeeman one, the sharp increasing values of $|h_a|$ due to the asymptotic approach to saturation leading to a Zeeman contribution more significant than the magnetostatic one. As a result, $|j_x^+|$ increases with $|h_a|$ until saturation.

In the frame of our modeling, the stage IV is not observed, the asymptotic approach to saturation being not rendered, due to the crude simplifications characteristic of our analytic approach, leading to $j_x^D = h_a$ and thus a saturating field equal to 1. For this reason, we restrict our simulations to the arbitrary interval $|h_a| < 0.95$.

2. Coercive case

A coercive behavior, corresponding to $k_i^H = 2$, is pictured on Fig. 10 for comparison with the anhysteretic preceding case. An interesting characteristic of local loops is the asymmetry featured by increasing and decreasing branches, as evidenced looking to the different values of remanences

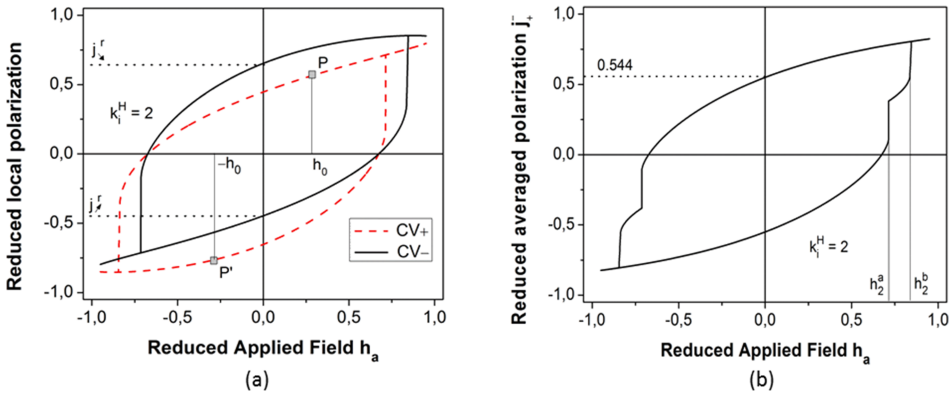

FIG. 10. Local coercive loops characteristics of CVHs featuring $k_i^H = 2$ (b). Corresponding averaged coercive loop.

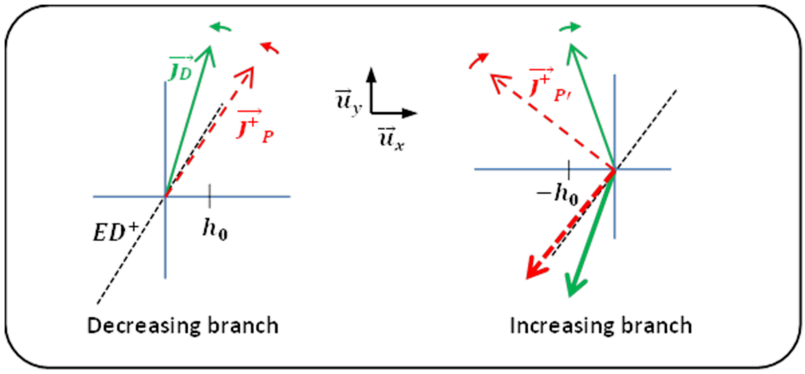

FIG. 11. Illustration of the interplay of the local polarization and the polarization of the surrounding domain explaining the asymmetry featured by local loops. Letters P and P' refer to points P and P' indicated on the local loop featured by a CVH+, as illustrated on Fig. 10a.

or critical fields, i.e., considering for instance the loop associated to CVH− : $\left|h^j_{\downarrow}\right| = h^a_2 = 0.72 \quad h^j_{\uparrow} = h^b_2 = 0.84 \quad j^r_{\downarrow} = 0.655 \quad j^r_{\uparrow} = -0.44$
where arrows refer to the increasing and decreasing branches.

This is explained looking again to magnetostatic interactions, controlled by $\vec{j_D}$. Figure 11 illustrates this question, dealing with a CVH+, looking to the peculiar situation of points P (decreasing branch) and P' (increasing branch) corresponding to $h_a = \pm h_0$ indicated on Fig. 10a. As illustrated on Fig. 11 by bold vectors, the local polarization $\vec{j_+}(P')$ would be symmetrical of $\vec{j_+}(P)$ if the polarization of the environment was fulfilling this property too, according to Curie's principle, i.e. $\theta_D(P') = \theta_D(P) + \pi$. This is not the case, $\theta_D(P')$ equaling $= \pi - \theta_D(P)$. As a result, the absolute value of the x component of $\vec{j_+}(P')$ is much greater than the one of $\vec{j_+}(P)$. The symmetry is of course restored looking to the averaged loop, as shown on Fig. 9b, the asymmetry featured by CVHs− compensating the one of CVHs+, but even at this scale, the memory of the local asymmetry is present, revealed by the two levels of irreversibility h^a_2 and h^b_2.

According to this explanatory framework, the asymmetry will be stronger the relative pound of magnetostatic interactions stronger is. This is illustrated on Fig. 12a, simulating the case $k^H_i = 1$, the local loop corresponding to CVHs− being not pictured to preserve clarity. Compared to Fig. 10a, the strengthening of the asymmetric character is spectacular, illustrating the sensitivity of the resulting loop to values of parameters when the energetic compromise involves contributions of comparable magnitudes.

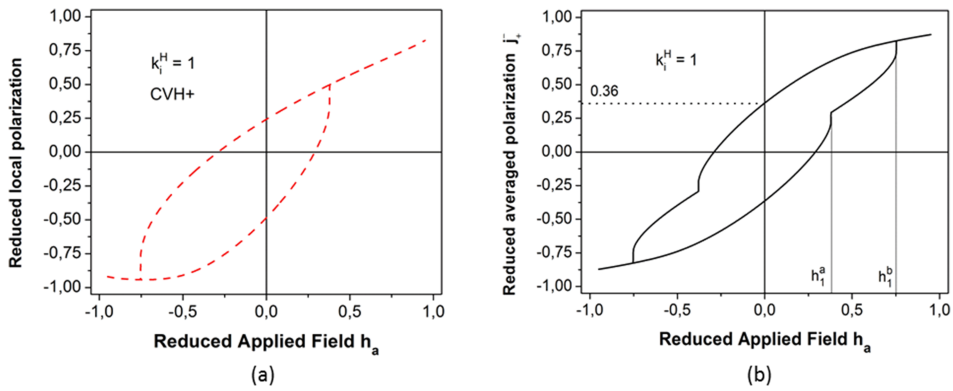

FIG. 12. (a): Illustration of the interplay between magnetostatic interactions and local anisotropy on the resulting asymmetry featured by ascending and descending branches of a local loop. The relatively small value $k^H_i = 1$ yields to an asymmetry much more pronounced than in the case $k^H_i = 2$ pictured on Fig. 10a. (b) Compensation of asymmetries looking to the averaged polarization (= considering the contribution of CVH− together with the one of CVH+).

D. Impact of CVHs at the macroscopic scale

To simulate the impact of CVHs on the macroscopic loop, the continuous distribution of k_i^H should be rendered. We simplify, choosing arbitrary 3 CVHs type of same pound for discretizing the distribution of hardnesses, i.e. ${}^{\alpha}k_i^H = 2$, ${}^{\beta}k_i^H = 1.5$ and ${}^{\gamma}k_i^H = 1$. The resulting averaged loop (= mixing those 3 contributions) is plotted on Fig. 13a.

Denoting z the CVHs volumetric part, the macroscopic polarization j_m obeys:

$$j_m(h_a) = (1-z)\, h_a + j_{av}^H(h_a) z \tag{35}$$

z is determined matching the experimental remanence j_r^{ex} with the simulated one $j_{H\,r}^{av} = 0.46$ (indicated on Fig. 13a). In the case of the sample pictured on Fig. 1, $j_r^{ex} = 0.0265$. This leads to $z_{16} = 5,76\%$, the subscript referring to the corresponding experimental value of K_u. The CVHs are clearly minority, in accordance with our hypothesis.

As mentioned at the beginning of Sec. III, CVHs were introduced for accounting coercivity or equivalently hysteretical character of the macroscopic loop. It is obvious that the narrow elongated look featured by the experimental loop pictured on Fig. 1b does not allow an easy characterization of this specific aspect, retaining the conventional graphical representation $j_m(h_a)$. It is so preferable to get rid of the anhysteretic skeleton. Facing this problem, it is considered in Ref. 7 the hysteretic component of the field $h_{hy}(j_m) = \left(h_a^{\uparrow}(j_m) - h_a^{\downarrow}(j_m)\right)/2$. The entrance variable being the polarization, this involves interpolating excitation fields. Remembering that data were at first interpolated with respect to polarizations (cf. Sec. III C), a loss of accuracy may occur due to successive interpolating operations, especially in regions associated to fronts. To avoid this problem, we propose here an equivalent alternative, retaining, as for local investigations, h_a as entrance variable: following Ref. 23, we so focus on the hysteretic component j_{hy} of the macroscopic polarization, j_{hy} obeying

$$j_{hy}(h_a) = \left(j_m^{\downarrow}(h_a) - j_m^{\uparrow}(h_a)\right)/2 \tag{36}$$

With (35), this simply yields to

$$j_{hy}(h_a) = \left(j_H^{av\downarrow}(h_a) - j_H^{av\uparrow}(h_a)\right) y/2 \tag{37}$$

The resulting j_{hy} curve is plotted (bold red) on Fig. 13b, and compared to two experimental curves: the hysteretic polarization j_{hy}^{16} obtained from the sample illustrated on Fig. 1, featuring $K_u = 16.2\, J/m^3$ (black continuous), and j_{hy}^{12} obtained from the sample illustrated on Fig. 1,[7] featuring $K_u = 12.1\, J/m^3$ (black dashed). In this last case, the reduce remanence equals 0.0285. This impacts the volumic part of CVHs, leading to $z_{12} = 6,2\%$ instead of $z_{16} = 5,76\%$ (considering the same distribution of CVHs, indexed on the value of K_u). To facilitate the comparison, j_{hy}^{12} has been renormalized, actual values being multiplied by j_r^{16}/j_r^{12} for equaling the amplitude of the corresponding curve (black dashed) with

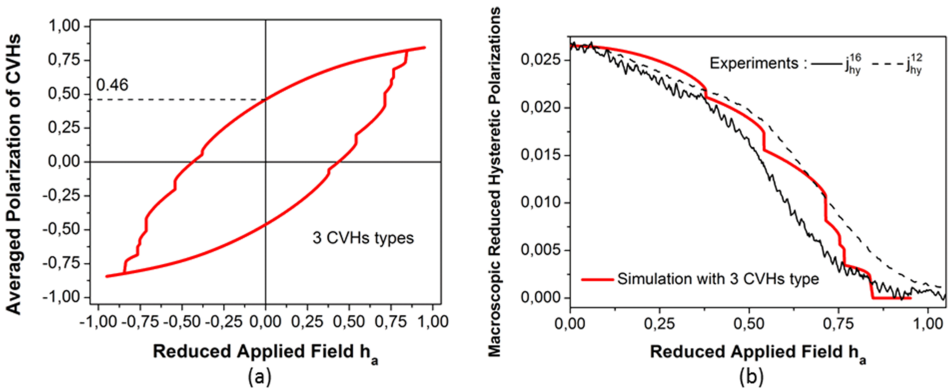

FIG. 13. (a): Averaged loop relative to the distribution of CVHs, i.e. ${}^{\alpha}k_i^H = 2$, ${}^{\beta}k_i^H = 1.5$ and ${}^{\gamma}k_i^H = 1$ with equal pounds. (b): resulting macroscopic hysteretic component of the polarization (magenta), compared with experimental curves ($K_u = 16.2\, J/m^3$, $K_u = 12.1\, J/m^3$).

others. From this, it is concluded that the postulated distribution of CVHs used for simulating is in qualitative agreement with experimental results.

IV. CONCLUSION

The simulations reported concern nanocrystalline soft ribbons featuring transverse loops. They are based on an analytical minimization of the total energy, made of Zeeman, anisotropic, and magnetostatic contributions, evaluated at the scale of individual CVs. Particular care is brought to the description of the magnetostatic interactions, modelled in the frame of a mean field theory.

The solving of equations show that majority CVs obeying the RAM explain well the domain pattern but one has to consider another kind of CVs, minority, featuring a magnitude of local uncoherent anisotropy K_i comparable to K_u, to account for the hysteretic character.

These investigations are very general and not addressed to the specific loops chosen for illustrating.

H_c reflecting the contribution of minority CVs, its use, in the context of transverse loops, as an experimental parameter reflecting the RAM, seems to be somewhat questionable.

The origin of the "hard" CVs is an opened question. In the case of transverse field annealing, a residual uncoherent magnetoelastic anisotropy could result from external stress applied during annealing.[7] Our own experimental investigations concerning field annealing, dealing with stress induced anisotropy, the evolution of coercivity with K_u reported in Ref. 6 should allow fruitful complementary experimental confrontation for modeling.

Numerous simplifications, inherent to the analytic approach, have been applied, dealing for instance with the uniaxial character of the uncoherent anisotropy or its 2D treatment, or the absence of hard CVs in the description of the environment of a given CV. The toughest problem is probably the assumption of an isotropic susceptibility χ for describing the equivalent homogeneous medium surrounding a peculiar CV, and the subsequent magnetostatic interactions. This crude simplification is probably responsible for the impossibility to simulate the asymptotic approach to saturation. This interpretation is reinforced by preliminary advanced modeling, simulations restoring the asymptotic behavior when the anisotropic character of χ is taken into account. This will be the subject of a future publication.

ACKNOWLEDGMENTS

This work was supported in part by the "Association Nationale de la Recherche et de la Technologie" (convention CIFRE 2015/1098).

APPENDIX

We consider a population of CVHs featuring an intrinsic uniaxial anisotropy of amplitude K_i with randomly distributed intrinsic Easy Directions in a plane, superimposed on a coherent uniaxial anisotropy of amplitude K_u and easy direction ED_{Ku} in the same plane. The objective of this appendix is to provide an analytic estimation of the mean deviation $\langle\varepsilon\rangle$ of the ED featured by the resulting effective anisotropy with respect to ED_{Ku} as a function of K_i/K_u, starting from the 3D simulations reported by Flohrer et al.[9]

In Ref. 9, K_i was attributed to the RAM, however simulations do not require any hypothesis about the origin of K_i. The results can so be reused in a more general context. We'll do it focusing on the asymptotic values featured by $\langle\varepsilon\rangle$ in the limit $K_i \gg K_u$: the mean deviation is thus entirely determined by the random distribution of intrinsic Easy Directions, $\langle\varepsilon\rangle_{lim}$ obeying

$$\langle\varepsilon\rangle_{lim}^{3D} = \int_0^{\pi/2} \varepsilon \sin\varepsilon d\varepsilon = 1 \text{ rad} \tag{A1}$$

$$\langle\varepsilon\rangle_{lim}^{2D} = \frac{2}{\pi}\int_0^{\pi/2} \varepsilon\, d\varepsilon = \frac{\pi}{4} \text{ rad} \tag{A2}$$

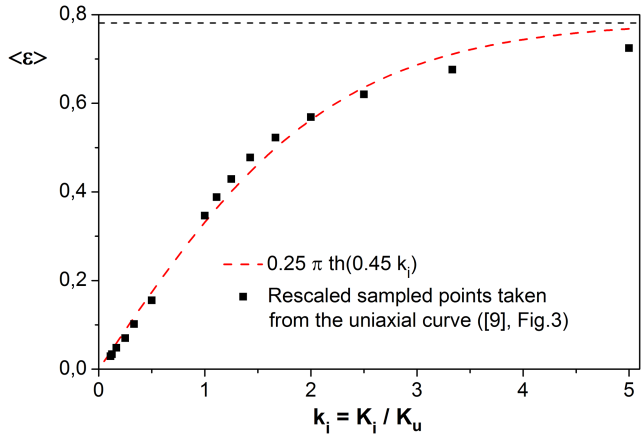

FIG. 14. Evolution of the average orientation of the ED for randomly oriented individual EDs with uniaxial anisotropy constant K_i and a superimposed uniform uniaxial anisotropy K_u.

We'll so adapt the 3D simulations of Flohrer et al to the 2D context by a simple linear correction carried out for matching the simulated asymptotic value $\langle\varepsilon\rangle_{lim}$ to the 2D situation, multiplying thus by $\langle\varepsilon\rangle_{lim}^{2D}/\langle\varepsilon\rangle_{lim}^{3D} = \pi/4$ the values $\langle\varepsilon\rangle$ taken from Ref. 9, Fig. 3, uniaxial curve. The resulting sampled points are plotted on Fig. 14 and fitted by the law

$$\langle\varepsilon\rangle = 0.25\,\pi \tanh 0.45 k_i \tag{A3}$$

[1] G. Herzer, *Amorphous and Nanocrystalline soft magnets*, ed. George C. Hadjipanayis, Nato ASI Series (Series E Vol. 338), Kluwer Academic Publishers (Dordrecht/Boston/London) 1997.
[2] S. Florer, R. Schäfer, C. Polak, and G. Herzer, "Interplay of uniform and random anisotropy in nanocrystalline soft magnetic alloys," Acta Materalia **53**, 2937–2942 (2005).
[3] R. Madugundo, O. Geoffroy, T. Waeckerle, B. Frincu, S. Kodjikian, and S. Rivoirard, "Improved soft magnetic properties in nanocrystalline FeCuNbSiB Nanophy® cores by intense magnetic field annealing," J. Magn. Mag. Mat. **422**, 475–478 (2017).
[4] F. Alves, F. Simon, S. N. Kane, F. Mazaleyrat, T. Waeckerlé, T. Save, and A. Gupta, "Influence of rapid stress annealing on magnetic and structural properties of nanocrystalline $Fe_{74.5}Cu_1Nb_3Si_{15.5}B_6$ alloy," J. Mag. Mag. Mater. **294**, e141 (2005).
[5] T. Waekerlé, T. Save, and A. Demier, "New stressed and continuously annealed low nanocrystalline FeCuNbSiB cores for watt-hour-metering or differential mode inductance applications," J. Mag. Mag. Mater. **320**, e797–e801 (2008).
[6] G. Herzer, V. Budinski, and C. Polak, "Magnetic properties of FeCuNbSiB nanocrystallized by flash annealing under high tensile stress," Phys. Status Solidi B **248**(10), 2382–2388 (2011).
[7] N. Boust, O. Geoffroy, H. Chazal, and J. Roudet, "Modeling of hysteresis in FeCuNbSiB cores with transverse K_u," IEEE Trans. Magn. **53**(11) (2017).
[8] K. Suzuki, G. Herzer, and J. M. Cadogan, "The effect of coherent uniaxial anisotropies on the grain-size dependence of coercivity in nanocrystalline soft magnetic alloys," J. Magn. Mag. Mat. **177-181**, 949–950 (1998).
[9] G. Herzer, "Anisotropies in soft magnetic nanocrystalline alloys," J. Magn. Mag. Mat. **294**, 99–106 (2005).
[10] S. Flohrer and G. Herzer, "Random and uniform anisotropy in soft magnetic nanocrystalline alloys," J. Magn. Mag. Mat. **322**, 1511–1514 (2010).
[11] G. Herzer, "Nanocrystalline soft magnetic alloys," *Handbook of Magnetic Materials*, 10, Buschow (1997).
[12] H. Gengnagel and H. Wagner, "Magnetfeldinduzierte anisotropie an FeAl- und FeSi-einkristallen," Z. Angew. Phys. **8**, 174 (1961).
[13] O. Geoffroy, H. Chazal, Y. Yao, T. Waeckerle, and J. Roudet, "Modelization of superferromagnetism in soft nanocrystalline materials based on an accurate description of magnetostatic interactions," IEEE Trans. Magn. **50**, 1–4 (2014).
[14] C. Polak, M. Knobel, R. Grossinger, and R. Sato Turtelli, "The development of nanocrystalline $Fe_{73.5}Cu_1Nb_3Si_{13.5}B_9$: Magnetism and structural disorder," J. Magn. Mag. Mat. **134**, 1–12 (1994).
[15] K.-Y. Ho, X.-Y. Xiong, J. Zhi, and L.-Z. Cheng, "Measurement of effective magnetic anisotropy of nanocrystalline Fe-Cu-Nb-Si-B soft magnetic alloys," J. Appl. Phys. **74**(11), 6788 (1993).
[16] X.-Y. Xiong and K.-Y. Ho, "Annealing temperature dependence of effective magnetic anisotropy of Fe-Cu-Nb-Si-B nanocrystalline alloys," J. Appl. Phys. **77**(5), 2094–2096 (1994).
[17] C. Appino and F. Fiorillo, "Reversible magnetization processes in amorphous alloys," J. Magn. Mag. Mat. **133**, 107–110 (1994).
[18] L. Néel, "Relation entre la constante d'anisotropie et la loi d'approche à la saturation des ferromagnétiques," J. Phys. Rad. **9**, 193–199 (1948).
[19] L. Néel, "Bases d'une nouvelle théorie générale du champ coercitif," Ann. Univ. Grenoble **22**, 299–343 (1946).

[20] A. Chikazumi, *Physics of Magnetism*, John Wiley, 1964, p. 190.
[21] L. Onsager, "Electric moments of molecules in liquids," J. Am. Chem. Soc. **58**, 1486–1493 (1936).
[22] E. C. Stoner and E. P. Wolhfarth, "A mechanism of magnetic hysteresis in heterogeneous alloys," Phil. Trans. Roy. Soc. London, A **240**(826), 599–642 (1948).
[23] P. Allia, M. Coisson, M. Knobel, P. Tiberto, and F. Vinai, "Magnetic hysteresis based on dipolar interactions in granular magnetic systems," Phys. Rev. B **60**(17), 12207–12217 (1999).